Incommensurate monolayers of Archimedean tiling formed on a square lattice

2008 J. Phys.: Condens. Matter 20 494226

(http://iopscience.iop.org/0953-8984/20/49/494226)

J. Phys.: Condens. Matter **20** (2008) 494226 (15pp) doi:10.1088/0953-8984/20/49/494226

Incommensurate monolayers of Archimedean tiling formed on a square lattice

W Rżysko, A Patrykiejew and S Sokołowski

Department for the Modelling of Physico-Chemical Processes, MCS University, 20031 Lublin, Poland

E-mail: wojtekrzysko@gmail.com

Received 14 July 2008, in final form 16 August 2008
Published 12 November 2008
Online at stacks.iop.org/JPhysCM/20/494226

Abstract

By using Monte Carlo simulation we investigate the structure of monolayer films formed on the (100) plane of a face centered cubic crystal, being a lattice of square symmetry. It is demonstrated that besides the commensurate c(2 × 2) phase, different incommensurate structures develop. In particular, we concentrate on the formation of rather peculiar structure which exhibits Archimedean tiling (AT) of type (3^2.4.3.4). The mechanism leading to the formation of the AT phase is identified and it is shown that it develops via small displacements of adatoms from registry positions. It is shown that the stability of the AT phase depends on the misfit between the adsorbate and the surface lattice as well as on the properties of the surface corrugation potential. The AT phase may be stable in the ground state or develop at finite temperatures from the commensurate c(2 × 2) structure, via a sharp first-order phase transition. The AT phase remains stable over a certain temperature range, and then it undergoes a transition to either the partially ordered phase of square symmetry or the incommensurate floating phase of triangular symmetry. In both cases a further increase of temperature leads to the formation of a liquid-like phase.

1. Introduction

The monolayers of simple atomic adsorbates on crystalline solids are known to form differently ordered phases [1–4]. The actual structure of the adsorbed film depends on several parameters, such as the relative size of adsorbate atoms and the surface lattice unit cell, the strength of the surface potential, its corrugation and the symmetry of the surface lattice. Moreover, the external thermodynamic conditions (the temperature and the chemical potential) are of great importance and may induce phase transitions between differently ordered phases. In principle, the adsorbed phases can be grouped into the following three classes: (i) commensurate, (ii) different high-order commensurate and (iii) incommensurate phases [3, 4]. Park and Madden [5] proposed a simple geometric criterion allowing one to distinguish different orderings in adsorbed films. Namely, the unit lattice cell vectors of the adsorbate phase, $\boldsymbol{e}_1$ and $\boldsymbol{e}_2$, are related to the unit lattice cell vectors of the surface lattice, $\boldsymbol{a}_1$ and $\boldsymbol{a}_2$, by the following equation:

$$\begin{bmatrix} \boldsymbol{e}_1 \\ \boldsymbol{e}_2 \end{bmatrix} = \begin{bmatrix} \alpha_{11} & \alpha_{21} \\ \alpha_{21} & \alpha_{22} \end{bmatrix} \begin{bmatrix} \boldsymbol{a}_1 \\ \boldsymbol{a}_2 \end{bmatrix}. \tag{1}$$

The commensurate structures correspond to integer values of the determinant $\det[\alpha_{ij}]$. The situations in which $\det[\alpha_{ij}]$ is a rational number correspond to the high-order commensurate phases, with only a fraction of adatoms located directly over the adsorption sites, i.e., over the minima of the adsorbate–solid interaction potential. Of course, the surface potential has the symmetry properties determined by the lattice structure of the crystal surface. Several examples of such high-order commensurate phases were observed in real systems [6–9]. Finally, whenever the determinant $\det[\alpha_{ij}]$ is an irrational number, the adsorbed phase is considered as incommensurate with the substrate surface lattice. The criterion of Park and Madden applies only to the so-called floating incommensurate phases and fails to describe incommensurate phases of domain wall structure [10]. In such cases the incommensurate phase is composed of large commensurate domains separated by walls which may have different structure, thickness, density and orientation [10, 11]. Both the commensurate and the high-order commensurate structures are periodic and have the symmetry properties determined by the symmetry of the underlying substrate surface lattice. On the other hand, the

structure of floating incommensurate phases is dominated by the interaction between adsorbed atoms and usually exhibits triangular symmetry. Of course, the surface corrugation potential introduces distortions to triangular ordering and often leads to the well known effect of epitaxial rotation [12–14]. The rotation of the adsorbed layer lattice with respect to the substrate lattice allows the system to reach a state of lower free energy.

The results of Monte Carlo simulation reported in our recent works [15, 16] have demonstrated that monolayer films formed on a square lattice of sites can order into a rather exotic phase in which every adatom has five nearest neighbors (see figure 1). The appearance of decagons, like that shown in figure 1, has led us to the conclusion that such monolayer films can be treated as an example of a two-dimensional quasi-crystal of decagonal ordering [17]. Shortly after our paper [16] was published we realized, however, that this ordered phase is periodic. This was also pointed out by Schmiedeberg and Stark in their comments [18] on our work. They have demonstrated that the structure obtained corresponds to the tiling known as Archimedean tiling (AT) of type $(3^2.4.3.4)$ [19]. This type of tiling has been found in layered crystalline structure of complex metallic alloys [20] known as Frank–Kasper phases [21], supramolecular micellar complex phases of organic dendrons [22], as well as in two-dimensional three-component copolymers [23]. The formation of such complex phases has never been observed experimentally as well as in computer simulation studies of simple monolayer films formed by atomic adsorbates.

The main objective of the present paper is to present the mechanism leading to the formation of AT and to elucidate the effects of periodic surface potential and misfit between the adsorbate and surface lattice on the stability of AT. The paper is organized as follows. In section 2 we present the model and Monte Carlo simulation methods used in our study. Then section 3 is devoted to the presentation of the mechanism leading to the formation of AT phase and to the discussion of the ground state behavior of the model. Then, in section 4 we present and discuss the results of Monte Carlo simulation carried out at finite temperatures. It is demonstrated that besides the commensurate c(2 × 2) and the AT phases, the adsorbed films can also form a floating incommensurate phase of triangular symmetry. Therefore, we also address the question of melting and disordering of the such triangularly ordered incommensurate films subjected to a corrugation potential of square symmetry.

2. The model and Monte Carlo methods

We consider a simple system of atoms interacting via the truncated Lennard-Jones potential

$$u(r) = \begin{cases} 4\varepsilon[(\sigma/r)^{12} - (\sigma/r)^6] & r \leqslant r_{\max} \\ 0 & r > r_{\max} \end{cases} \qquad (2)$$

with $r_{\max} = 3\sigma$, adsorbed on a model (100) plane of a face centered cubic (fcc) crystal. The atoms of a fluid interact with the substrate atoms via the Lennard-Jones potential as well.

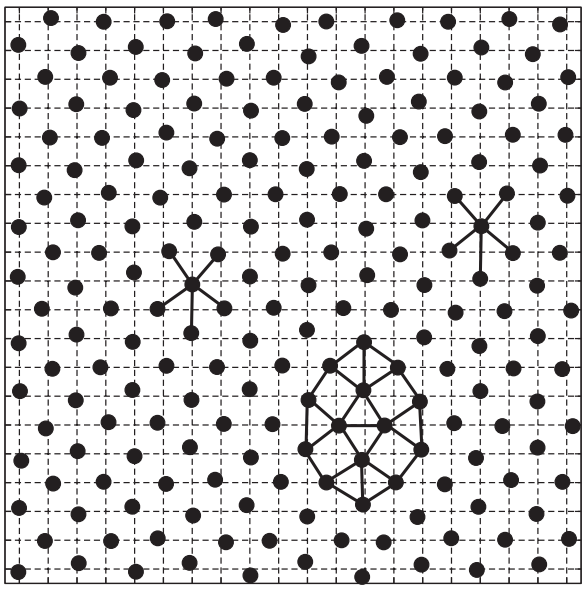

Figure 1. A snapshot of a configuration recorded at $T^* = 0.2$ for the monolayer film consisting of atoms of $\sigma^* = 1.34$ and the surface potential characterized by the parameters $\varepsilon^*_{\rm gs} = 1.0$ and $V_{\rm b} = 1.0$. The simulation cell of $L = 20$ was used. Crossing points of thin vertical lines mark the locations of the centers of surface lattice cells (surface potential minima) and the heavy solid lines show the AT structure.

The substrate surface is a square lattice of sites, which are separated by a finite potential barrier. Throughout this work we take the length of the surface lattice constant a as a unit of length and ε as a unit of energy.

The surface field is periodic in the directions parallel to the surface (x and y), and hence can be represented by the Fourier series [24]

$$v^*(z^*, \boldsymbol{\tau}^*) = \varepsilon^*_{\rm gs}\left[v_o(z^*) + V_{\rm b}\sum_{g\neq 0} v_g(z^*) f_g(\boldsymbol{\tau}^*)\right], \qquad (3)$$

where $z^* = z/a$ is the distance from the surface, $\boldsymbol{\tau}^* = (x^*, y^*)$ ($x^* = x/a$ and $y^* = y/a$) is the 2D vector specifying the position of an adatom over the surface lattice and the sum runs over different (non-zero) reciprocal surface lattice vectors. The Fourier coefficients $v_g(z^*)$ and the functions $f_g(\boldsymbol{\tau}^*)$ are given by analytic expressions [24]. The parameter $V_{\rm b}$ has been introduced in order to allow for changes of the periodic part of the surface potential [25]. As long as the parameter $V_{\rm b}$ is equal to unity the Fourier series (3) gives the same results as the direct summation of interactions between the adsorbate atom and the atoms of the substrate, provided that a sufficient number of terms in the sum over reciprocal lattice vectors have been taken into account.

In the case considered here of the surface being the (100) plane of an fcc crystal it is sufficient to use the first five non-zero reciprocal lattice vectors in order to obtain a potential of practically the same properties as the potential resulting from a direct summation of atom–atom interactions. We have considered several systems of adsorbate atoms characterized by σ^* ranging between 1.26 and 1.47, and by the surface potential with different values of $\varepsilon^*_{\rm gs}$ and $V_{\rm b}$.

The model has been studied by MC methods in the canonical ensemble using the parallel tempering technique [26, 27], which allows one to study a series of thermodynamic states, i.e., of different temperatures, in a single run. The method is very efficient and considerably reduces the number of MC steps needed to reach equilibrium, as well as to obtain reliable estimations of averages. A single MC step (MCS) consisted of N (N being the number of particles in the system) randomly chosen displacements of particles. The maximum displacement was adjusted during the run to keep the acceptance ratio at about 40%). The number of MCSs performed during a single run varied between 10^5 and 10^6 and a similar number of MCSs was used to equilibrate the system. Standard periodic boundary conditions were applied in the directions parallel to the surface and a hard reflecting wall placed at $z^* = 20$ was used to close the system from above. To facilitate finite size scaling analysis we have used simulation cells of the size $L \times L \times 20$, with L ranging between 12 and 60.

All canonical ensemble Monte Carlo simulations were performed for the fixed density of adsorbed film corresponding to a perfect commensurate c(2×2) structure in which half of all potential minima is occupied by adsorbate atoms. i.e., it was equal to 0.5 in the case of monolayer films. Of course, for large values of σ^* the stability of the commensurate c(2×2) phase is rather limited, since the adatom–adatom interaction becomes repulsive. Only when the surface potential is sufficiently strong and strongly corrugated it is possible to enforce the formation of the commensurate c(2×2) phase.

In some cases we have also used Monte Carlo methods in the grand canonical ensemble in order to determine adsorption–desorption isotherms, as well as to check whether it is possible to obtain AT phase when the dilute gas-like phase condenses into a dense monolayer film.

The internal structure of adsorbed films has been probed by the calculation of the bond-orientational order parameters [4, 28]

$$\Psi_k = \left\langle \left| \frac{1}{N_\mathrm{b}} \sum_{i \in l} \sum_{j \in l} \exp[\mathrm{i}k\phi_{ij}] \right| \right\rangle, \qquad k = 4, 6, 12, \quad (4)$$

that are suitable for detecting the formation of layers of square ($k = 4$) and hexagonal ($k = 6$) symmetry as well as the appearance of AT phase ($k = 12$). In the above equation, ϕ_{ij} is the angle between the 'bond' joining the nearest neighboring atoms i and j in the monolayer and the fixed reference axis, N_b is the number of such 'bonds', and $\langle \cdots \rangle$ means the averaging over the configurations generated during a MC run. The first-nearest neighbors of each adatom have been determined using the in-plane cutoff, defined as the location of the first minimum of the radial distribution function [29], while the extent of the first layer in the z direction has been determined using the density profiles.

In the case of a perfectly ordered AT phase the bond-orientational order parameter Ψ_{12} is equal to unity, Ψ_4 assumes low values, while $\Psi_6 = 0$. When a perfectly ordered commensurate c(2×2) phase is formed, both Ψ_4 and Ψ_{12} are equal to unity, while $\Psi_6 = 0$ again. Only in the case of a floating incommensurate phase of triangular symmetry is the bond-orientational order parameter Ψ_6 expected to reach values close to unity.

We have also monitored the Fourier transform of the local density in the monolayer film

$$|\rho_q| = \left\langle \left| \frac{1}{N_l} \sum_{i=1}^{N_l} \exp(-\mathrm{i}\boldsymbol{q} \cdot \boldsymbol{r}_i) \right| \right\rangle, \quad (5)$$

which allows us to probe the positional order corresponding to the presence of the assumed commensurate phase, characterized by the reciprocal lattice vector $\boldsymbol{q}$ [30, 31]. We have also calculated the susceptibilities ($\chi_\mathrm{op} = NkT[\langle \mathrm{op} \rangle^2 - \langle \mathrm{op}^2 \rangle]$) as well as the fourth-order 'Binder' cumulants [32] ($U_L = 1 - \langle \mathrm{op} \rangle^4 / 3\langle \mathrm{op}^2 \rangle^2$) conjugated to the above defined order parameters (op $= \Psi_k$ or $|\rho_q|$).

3. The formation of AT phase and the ground state properties of the model

From the snapshot shown in figure 1 it is evident that the development of AT phase results from rather small displacements of adsorbed atoms from registry positions. In order to obtain quantitative information about these displacements we have recorded the density distribution function, $\rho(\hat{\boldsymbol{\tau}}^*)$, mapped onto a single lattice cell ($\hat{\boldsymbol{\tau}}^* = \boldsymbol{\tau}^* - \mathrm{int}(\boldsymbol{\tau}^*)$), for different systems which exhibit the formation of AT phase. Figure 2 presents representative examples obtained for adatoms of $\sigma^* = 1.34$ and the surface potential characterized by $\varepsilon^*_\mathrm{gs} = 1.0$ and $V_\mathrm{b} = 1.0$, recorded at $T^* = 0.20$ for two different sizes of the simulation cell $L = 40$ (part (a)) and $L = 30$ (part (b)). One readily notes that the density distribution possesses four maxima, at the positions $(0.5 \pm \delta, 0.5)$ and $(0.5, 0.5 \pm \delta)$, with δ being roughly the same for the displacements along the two surface lattice symmetry axes (x and y). Comparing the density distributions in parts (a) and (b) of figure 2 one also notes that the peaks at the density distribution obtained for $L = 40$ are much sharper than those obtained for $L = 30$. From the inspection of density distribution functions obtained for different systems and different sizes of the simulation cell it follows that whenever the linear dimension of the simulation cell (L) is an integer multiple of 4 ($L = 16, 20, 24, \ldots$) the density distribution function looks like that depicted in figure 2(a), while for $L = 18, 22, 26, \ldots$ the density distributions look like that given figure 2(b). Of course, the linear dimension of the system has to be an even number to accommodate the commensurate c(2×2) structure in the simulation cell with periodic boundary conditions applied in both x and y directions.

Both, the inspection of snapshots and the above presented behavior of density distribution functions allow us to propose a mechanism leading to the development of AT phase, in which every adatom has five nearest neighbors. In an idealized situation, when the displacement of adatoms from registry positions leads to the structure in which all five nearest neighbors are at the same distance from the central atom, the pattern corresponding to a perfect AT is formed (see figure 3(a)). In order to transform the commensurate c(2×2)

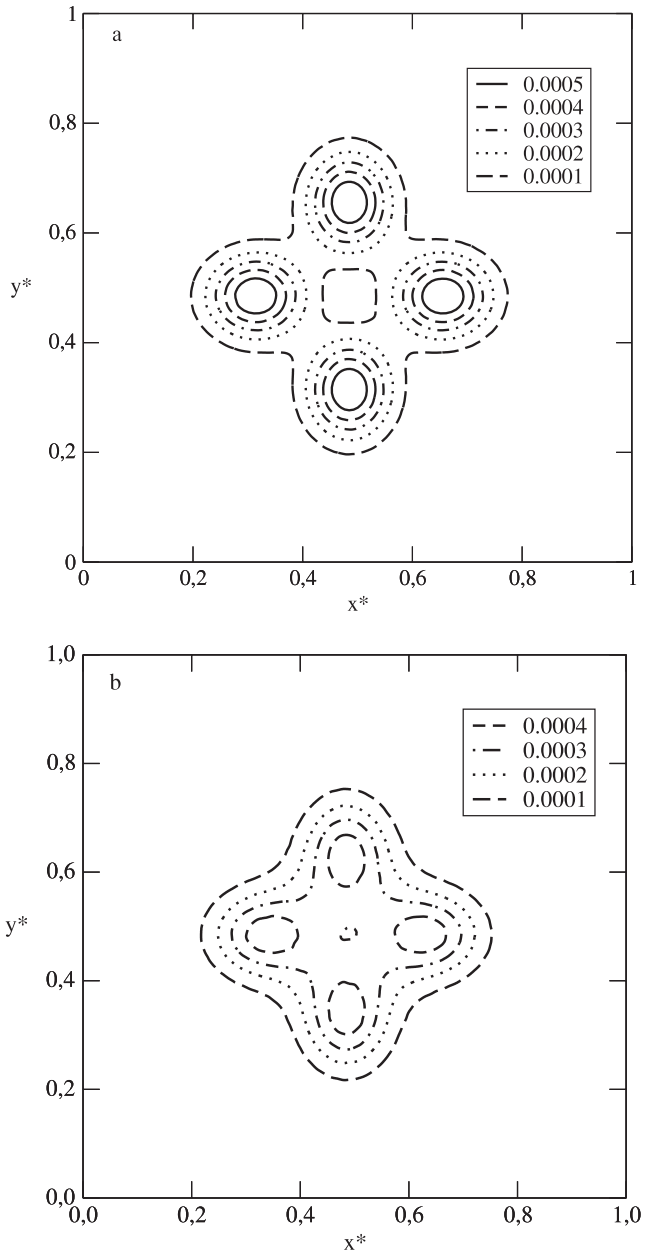

Figure 2. Contour maps of the density distribution functions $\rho(\hat{\boldsymbol{\tau}}^*)$, obtained at $T^* = 0.2$ for the monolayer film consisting of atoms of $\sigma^* = 1.34$ and the surface potential characterized by the parameters $\varepsilon^*_{\rm gs} = 1.0$ and $V_{\rm b} = 1.0$. Parts (a) and (b) correspond to $L = 40$ and 30, respectively.

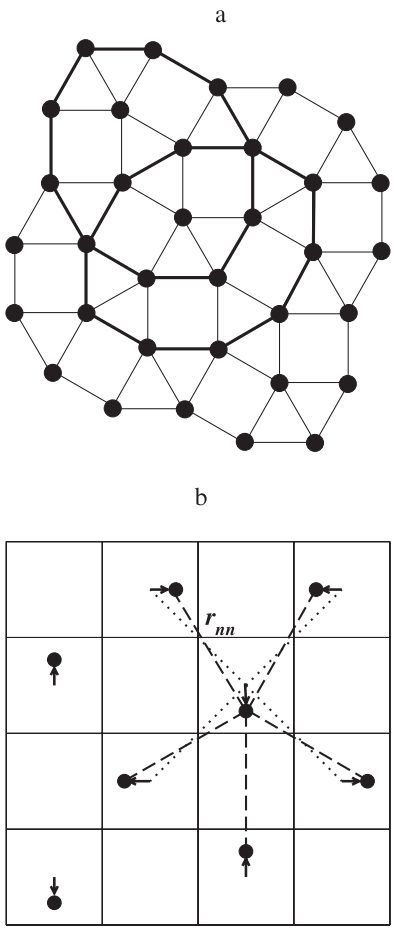

Figure 3. Part (a) shows a perfect AT. Part (b) represents a basic 4×4 unit lattice cell allowing us to construct AT on the lattice. The arrows show the displacement vectors applied to all atoms. Dotted and dashed lines represent the nearest neighbor distances in the commensurate and decagonally ordered phases, respectively.

structure of square symmetry into a perfect AT structure, one needs to consider a block of the size (4×4), i.e., consisting of 16 surface unit cells, and displace each atom by one of the vectors $(\pm\delta_o, 0)$ or $(0, \pm\delta_o)$ in a manner shown in figure 3(b). The length of the displacement vector, δ_o, can be readily obtained from a simple geometry and it is equal to $\delta_o = (\sqrt{3} - 1)/(\sqrt{3} + 1) \approx 0.2679$, while the distance between the nearest neighbors is equal to $r_{\rm nn} = 4/(\sqrt{3} + 1) \approx 1.464$. The construction given in figure 3(b) explains the observed differences in behavior of density distribution functions shown in figure 2 for the systems of linear dimension $L = 4k$ and $L = 4k + 2$ (k being a positive integer). Only in the case of $L = 4k$ do the periodic conditions correctly match the periodicity of AT structure.

The results of Monte Carlo simulations performed for different systems have demonstrated that the lengths of displacement vectors are different (smaller) than δ_o, so that the AT ordering is never exactly the same as that shown in figure 3(a). This observation can be explained by considering the ground state behavior of our model.

In the case of a perfectly ordered commensurate c(2×2) phase the potential energy (per atom) can be readily calculated and it is equal to

$$E_{\rm c} = 0.5 \sum_l n_l u(r_l^*) + v(\boldsymbol{\tau}^*_{\rm S}, z^*_{\rm min,S}), \qquad (6)$$

where n_l is the number of neighbors in the lth shell, located at the distance r_l^* from the central atom, $v(\boldsymbol{\tau}^*_{\rm S}, z^*_{\rm min,S})$ is the minimum value of the surface potential exactly over the center of a lattice unit cell ($\boldsymbol{\tau}^*_{\rm S} = (0.5, 0.5)$) and $z^*_{\rm min,S}$ is the location of the surface potential minimum with respect to the distance from the surface over the center of a lattice unit cell. In a similar fashion, one can calculate the potential energy (per atom) of the structure in which all atoms are displaced from

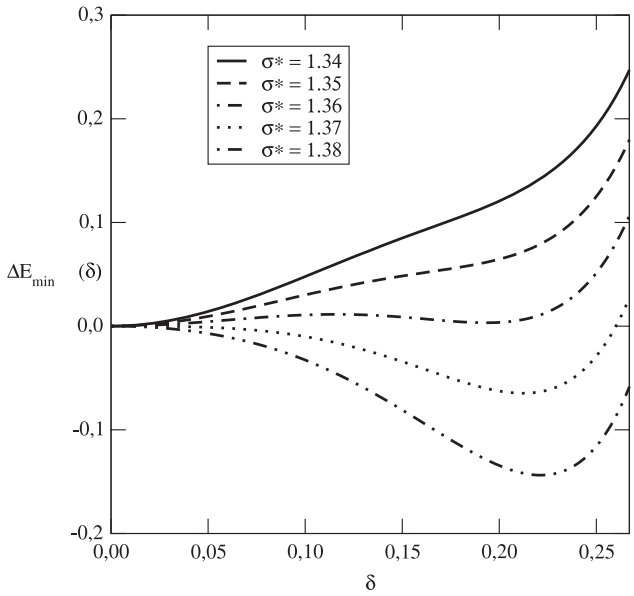

Figure 4. The difference $\Delta E_{\min}(\delta) = E_{\mathrm{AT}}(\delta) - E_{\mathrm{c}}$ versus δ for a series of systems characterized by different σ^* (shown in the figure) and the surface potential with $\varepsilon^*_{\mathrm{gs}} = 1.0$ and $V_{\mathrm{b}} = 1.0$.

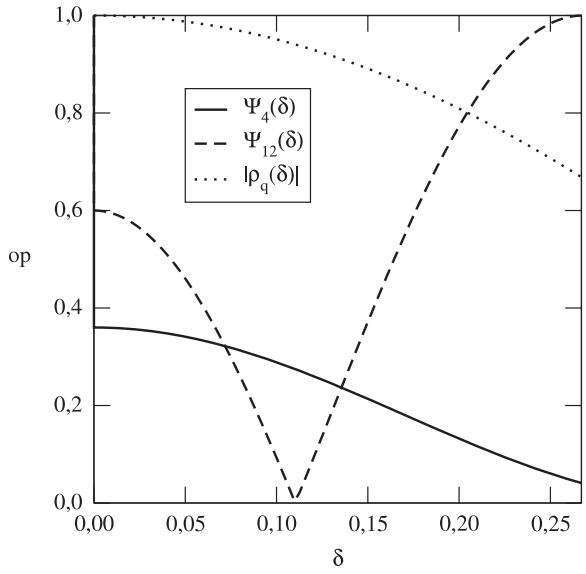

Figure 5. The order parameters Ψ_4, Ψ_{12} and $|\rho_q|$ plotted against the displacement δ in the ground state.

registry positions by the vectors $(\pm\delta, 0)$ and $(0, \pm\delta)$, for any $\delta \leqslant \delta_o$, and we have

$$E_{\mathrm{AT}}(\delta) = 0.5 \sum_l n_l u[r_l^*(\delta)] + v[\boldsymbol{\tau}^*(\delta), z^*_{\min,\delta}]. \qquad (7)$$

In the above $z^*_{\min,\delta}$ denotes the distance from the surface at which the surface potential reaches minimum for a given value of δ. Of course, as soon as the displacement δ is greater than zero the numbers of neighbors at different coordination shells (the numbers (n_l)) are different than for the commensurate phase. In fact, for any $0 < \delta \leqslant \delta_o$ the central atom has five first-nearest neighbors: four at the distance $\sqrt{2(1+\delta^2)}$ and one at the distance $2(1-\delta)$.

In the ground state, a stable structure is that of the lowest energy. Figure 4 presents examples of plots of the difference $\Delta E_{\min}(\delta) = E_{\mathrm{AT}}(\delta) - E_{\mathrm{c}}$ versus δ, obtained for a series of systems of different σ^* and characterized by the same values of $\varepsilon^*_{\mathrm{gs}} = 1.0$ and $V_{\mathrm{b}} = 1.0$. The results show that the systems with $\sigma^* = 1.34$, 1.35 and 1.36 are not likely to form the AT in the ground state. On the other hand, as soon as σ^* exceeds 1.36 the absolute minimum of the energy corresponds to the AT phase, though it is not perfectly ordered since the energy reaches its minimum value for $\delta < \delta_o$. The results given in figure 4 are quite consistent with our simulation results that will be discussed in section 4.

In figure 5 we present the plots of the bond-orientational order parameters Ψ_4, Ψ_{12} and of the order parameter $|\rho_q|$ versus the length of the displacement vector δ in the ground state. The bond-orientational order parameter $\Psi_{12} = 1.0$ for perfectly ordered commensurate and AT phases, Ψ_4 is equal to unity only for $\delta = 0$, i.e., for a perfect commensurate phase, while the bond-orientational order parameter Ψ_6 is equal to zero for any δ.

When the surface corrugation becomes weak enough the adsorbed film may also order into the triangularly ordered floating incommensurate phase, as was already observed in monolayers formed on square substrates [33]. Although the calculation of the potential energy of triangularly ordered phase formed over a square lattice of sites is a nontrivial problem, nevertheless we can obtain a rough estimate by considering an idealized situation. Namely, we assume that the film forms a perfect triangular lattice floating above the substrate surface. Under such conditions, we can assume that, on average, the surface field felt by an adatom is equal to the surface potential averaged over the entire surface, i.e., it is equal to $\varepsilon^*_{\mathrm{gs}} v^*_o(z^*)$ (cf equation (3)), so that the total potential energy (per atom) is equal to

$$E_{\mathrm{TR}} = 0.5 \sum_l n_l u(r_l^*) + \varepsilon^*_{\mathrm{gs}} v_o(z^*) \qquad (8)$$

where the sum runs over all shells of neighbors of a perfect triangular lattice. In order to obtain the distances r_l one needs to minimize the fluid–fluid interaction energy with respect to the first-nearest neighbor distance only [4].

The above procedure does not lead to an exact solution of the problem, since the triangular ordering may be, and usually is, distorted by the corrugation potential. Besides, the density of a perfect triangular phase is different from the densities of both the commensurate c(2×2) and the AT ordered phases. When the canonical ensemble Monte Carlo simulation is performed for the system of density equal to the density of the commensurate phase different situations may emerge. For small adsorbate atoms, voids are expected to appear as soon as the triangular ordering sets in. On the other hand, when adatoms are sufficiently large the promotion of the second layer is likely to accompany the formation of incommensurate phase of triangular symmetry. The first situation is illustrated by the snapshot given in figure 6, obtained for adatoms of $\sigma^* = 1.27$. This figure also shows that the triangular phase is rotated with respect to the symmetry axes of the surface lattice. Our simple model ground state calculations do not

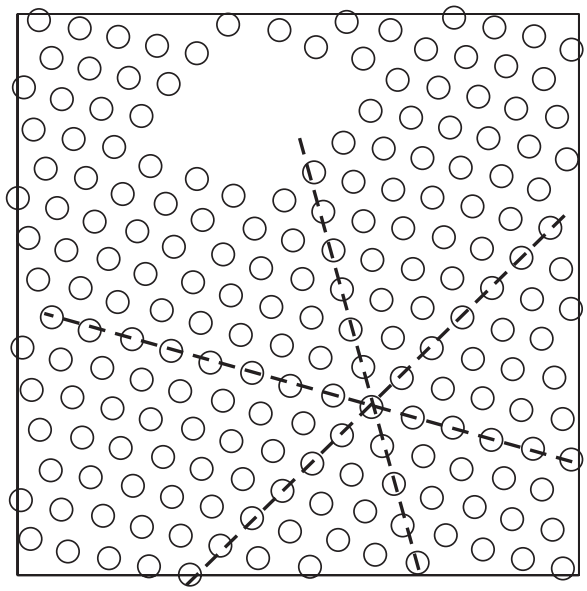

Figure 6. A snapshot recorded for the system with $\sigma^* = 1.27$, $\varepsilon^*_{gs} = 1.0$ and $V_b = 0.5$ at $T^* = 0.002$.

involve the effects due to epitaxial rotation. Having all the above mentioned shortcomings in mind we can nevertheless evaluate the energy of the triangular phase and obtain a rough estimation of its stability region. In all cases shown in figure 4 the difference $E_{TR} - E_c$ is greater than zero and hence an incommensurate phase of triangular ordering is not expected to appear at $T = 0$.

We have carried out the ground state calculations for several systems and our primary aim was to estimate the interval of σ^* over which the AT ordering can appear at $T = 0$. From the results obtained it follows that the AT phase is possible at $T = 0$ only for adatoms of $\sigma^* \in [1.29, 1.44]$. Figure 7 presents representative examples of the ground state calculations for the systems with $\sigma^* = 1.28$, 1.29, 1.44 and 1.45. This figure also shows that in all cases the energy of AT phase reaches a minimum for the displacement (δ) smaller that δ_o, in agreement with Monte Carlo simulation results.

Since the development of AT phase occurs via relatively small displacements of adatoms from the centers of surface unit cells, the height of the potential barrier between adjacent minima $V^*_D = v(z^*_{SP}, \boldsymbol{\tau}^*_{SP}) - v(z^*_S, \boldsymbol{\tau}^*_S)$, where SP denotes the saddle point position, is not likely to be the parameter controlling the ability of atoms to displace from registry positions. It is rather controlled by the curvature of the surface potential near the minimum. Since the adatom displacements occur along the symmetry axes of the surface lattice, one can characterize the curvature of the surface potential by considering a simple one-dimensional situation and approximate the surface potential by the harmonic potential

$$v^*_{har}(x^*) = v^*_{min} + k_x(x^* - 0.5)^2 \tag{9}$$

where k_x is the force constant given by

$$k_x = \frac{1}{2}\left[\frac{\partial^2 v^*(z^*, x^*, y^*)}{\partial x^{*2}}\right]_{z^*=z^*_S, \boldsymbol{\tau}^*_S}. \tag{10}$$

Of course, the displacement along the y axis leads to the same result due to the symmetry of the surface lattice. The second derivative of the surface potential with respect to x^* can be readily obtained from the known functions $f_g(\boldsymbol{\tau}^*)$ (see

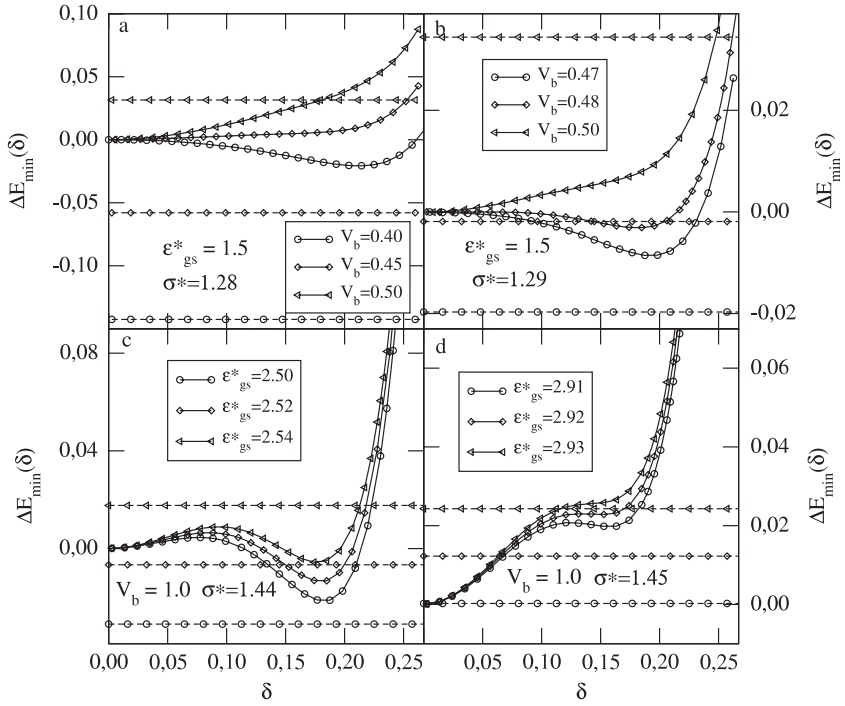

Figure 7. The results of ground state calculations for the systems characterized by $\sigma^* = 1.28$ (part (a)), 1.29 (part (b)), 1.44 (part (c)) and 1.45 (part (d)). The applied values of ε^*_{gs} and V_b are shown in the figure. Dashed horizontal lines decorated with symbols correspond to the energy difference between the triangularly ordered and the commensurate phases.

equation (3)). The force constant k_x is a direct measure of the curvature of the surface potential near the minimum. It should be noted that the force constant k_x is proportional to the product $\varepsilon^*_{gs}V_b$, and hence it is also proportional to the potential barrier for diffusion (V^*_D). Of course, k_x also depends on the size of adsorbate atoms and decreases with σ^*. For example, assuming that $\varepsilon^*_{gs} = 1.0$ and $V_b = 1.0$, we obtain $k_x \approx 8.546$ for $\sigma^* = 1.26$ and $k_x \approx 7.193$ for $\sigma^* = 1.46$. Of course, the potential barrier for diffusion also decreases with σ^* and we have $V^*_D \approx 1.212$ for $\sigma^* = 1.26$ and $V^*_D \approx 1.039$ for $\sigma^* = 1.46$.

The displacement of adatoms along the x axis, as well as along the y axis, is also accompanied by change of the distance from the surface. Therefore, also the curvature of the surface potential along the z axis, measured by the force constant k_z,

$$k_z = \frac{1}{2}\left[\frac{\partial^2 v^*(z^*, x^*, y^*)}{\partial z^{*2}}\right]_{z^*=z^*_S, \boldsymbol{\tau}^*_S}, \tag{11}$$

is of importance. The force constant k_z is given by

$$k_z = \varepsilon^*_{gs}\left\{\frac{1}{2}\left[\frac{\partial^2 v^*_o(z^*)}{\partial z^{*2}}\right]_{z^*=z^*_S} + V_b\sum_g\left(\frac{1}{2}\left[\frac{\partial^2 v^*_g(z^*)}{\partial z^{*2}}\right]_{z^*=z^*_S} f_g(\boldsymbol{\tau}^*_S)\right)\right\} \tag{12}$$

and contains the term proportional to ε^*_{gs} and the term proportional to the product $\varepsilon^*_{gs}V_b$. It appears, however, that the periodic part of the surface potential has only a small effect on k_z. In fact the force constant k_z changes by less than 5% when the corrugation parameter changes between zero and unity (see figure 8).

In the following section we shall demonstrate that the two curvatures, k_x and k_z, have a great influence on the structure of adsorbed films and, in particular, on the formation and stability of the phase which exhibits the AT ordering.

4. Results of finite temperature Monte Carlo simulation and discussion

It was demonstrated in [16] that in the systems ordering into the commensurate c(2 × 2) phase at $T = 0$, the AT phase can nevertheless appear at finite temperatures, via the first-order phase transition. At finite temperatures, the system free energy strongly depends on the entropy and hence the AT phase may be stabilized by this entropic contribution. Therefore, we have checked whether the AT phase can develop at finite temperatures in the systems of adatoms of $\sigma^* < 1.29$, and considered two series of systems with $\sigma^* = 1.27$ and 1.28.

From the ground state calculations for the systems with $\sigma^* = 1.27$, $\varepsilon^*_{gs} = 1.0$ and different values of the corrugation parameter, V_b, it follows that monolayer films of triangular ordering are stable whenever V_b is lower than about 0.665. Monte Carlo calculations performed at finite temperatures have confirmed this prediction very well. In particular, the annealing runs with the starting configuration corresponding to a perfect commensurate film and the corrugation parameter equal to and lower than $V_b = 0.65$ have been found to lead to

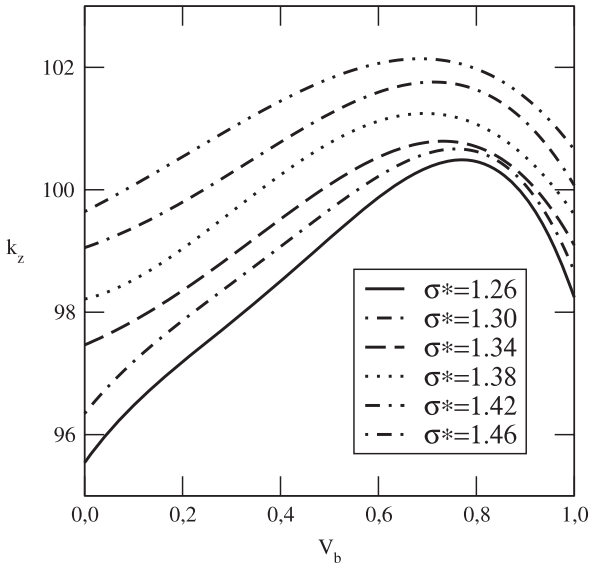

Figure 8. The force constant k_z versus the corrugation parameter V_b for a series of systems with $\varepsilon^*_{gs} = 1.0$, $V - B = 1.0$ and different σ^* (shown in the figure).

the formation of triangularly ordered structures at sufficiently high temperatures (cf figure 6). Subsequent freezing runs have always demonstrated that triangularly ordered structure remains stable even at very low temperatures, in agreement with the results of ground state calculations, and demonstrated that the commensurate phase, used as a starting configuration, is not a stable state. On the other hand, both annealing and freezing runs performed for the systems with $V_b \geqslant 0.675$ led to the recovery of the commensurate phase at low temperatures. This is demonstrated in figure 9, which presents the changes of the bond-orientational order parameters Ψ_4 and Ψ_6 with temperature for a series of systems characterized by different values of the corrugation parameter. The freezing runs have always shown the formation of triangularly ordered phase at low temperatures. We have also checked that the potential energy of the film reaches lower values for the triangularly ordered phase at the temperatures approaching zero.

The systems with $V_b \geqslant 0.7$ do not show the formation of AT phase at all. The changes of the bond-orientational order parameters shown in figure 9 suggest that the formation of AT phase may be possible for the system with $V_b = 0.675$. Indeed, a direct inspection of snapshots recorded for systems of different size of the simulation cell, with $L = 32$ and 40, has demonstrated that the AT develops (see figure 10).

The development of AT phase was not observed when the same system was studied by grand canonical Monte Carlo simulation. For example at the temperature of 0.3 we have observed the formation of 'mixed structures', consisting of commensurate domains of square ordering and incommensurate domains of triangular ordering. An increase of temperature to 0.4 has led to the formation of quite well developed triangular order in the film. Thus, we should conclude that the AT phase is not a stable state for this system.

A further increase of V_b to 0.7 also leads to small displacements of adatoms, but neither the density distributions

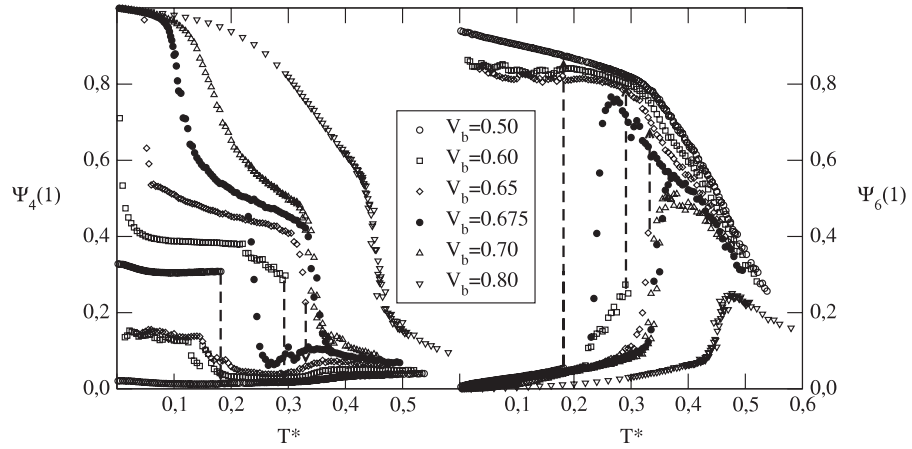

Figure 9. Temperature changes of the bond-orientational order parameters Ψ_4 (left panel) and Ψ_6 (right panel) for the systems characterized by $\sigma^* = 1.27$, $\varepsilon^*_{gs} = 1.0$ and different values of the corrugation parameter (shown in the figure). Vertical dashed lines mark the jumps of order parameters during the annealing runs for the systems with $V_b \leqslant 0.65$.

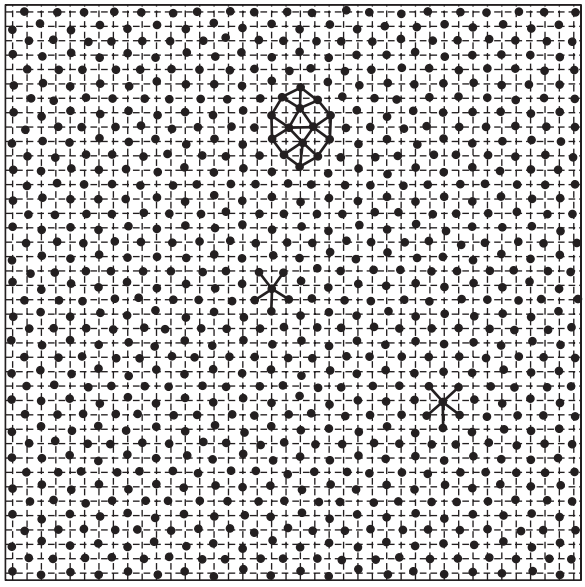

Figure 10. A snapshot of configuration recorded at $T^* = 0.128$ for the monolayer film consisting of atoms of $\sigma^* = 1.27$ and the surface potential characterized by the parameters $\varepsilon^*_{gs} = 1.0$ and $V_b = 0.675$. The simulation cell of $L = 40$ was used. Crossing points of thin vertical lines mark the locations of the centers of surface lattice cells (surface potential minima) and the heavy solid lines show that adatoms have five nearest neighbors and the distorted AT structure.

nor the snapshots allow us to conclude that the AT appears. Of course, the AT ordering does not appear for still higher values of V_b.

The formation of well developed triangular ordering in the systems with $\sigma^* = 1.27$ and low values of the corrugation parameter allow us to address the problem of the nature of the melting transition of triangular incommensurate pseudo-two-dimensional phase subjected to an external field of square symmetry. From the Nelson–Halperin renormalization group calculations [34] it follows that in strictly two-dimensional systems the melting transition should occur via two second-order phase transitions. The first transition, leading to the disappearance of quasi-long-range positional order, is due to unbinding of pairs of dislocations [35], but the system is expected to retain quasi-long-range orientational order. Then the second transition, at a higher temperature, is expected to take place, and in the particular case of a substrate of square lattice symmetry it is predicted to be an Ising-like transition. The substrate field then presents a 12-fold symmetric potential, which acts like an Ising perturbation on the bond-orientational order parameter Ψ_6. At the temperatures above the transition point the bond-orientational order parameter Ψ_6 is expected to approach zero.

In order to investigate the melting of such triangular incommensurate solid-like phases we have considered the system characterized by $\varepsilon^*_{gs} = 1.0$ and $V_b = 0.5$ and performed the canonical as well as grand canonical ensemble simulations for different sizes of the simulation cell, L, ranging between 20 and 60. The results obtained from the canonical ensemble simulation, carried out at the density corresponding to a perfect commensurate c(2 × 2) phase ($\rho = 0.5$), quite clearly demonstrate that there are two phase transitions present (see figure 11). The first transition, which takes place at the temperature of about 0.38 is manifested by the presence of a very sharp specific heat maximum of the height depending on the simulation cell size (see figure 11(a)). It is also accompanied by a small drop of the bond-orientational order parameter Ψ_6 (figure 11(b)) and by a weak anomaly of its susceptibility (figure 11(c)). This anomaly becomes visible only for sufficiently large systems of $L \geqslant 40$. The presence of a pronounced specific heat anomaly does not contradict the defect mediated melting theory. This theory predicts only that the heat capacity does not diverge at the melting point. On the other hand, the theory does not say anything about the width or height of the heat capacity peak at the melting temperature. Unfortunately, the quality of our heat capacity data is not good enough to apply finite size scaling and decide whether the specific heat peak diverges upon the increase of the simulation cell or not.

The defect mediated melting theory is expected to be valid for strictly two-dimensional systems, while our system is not

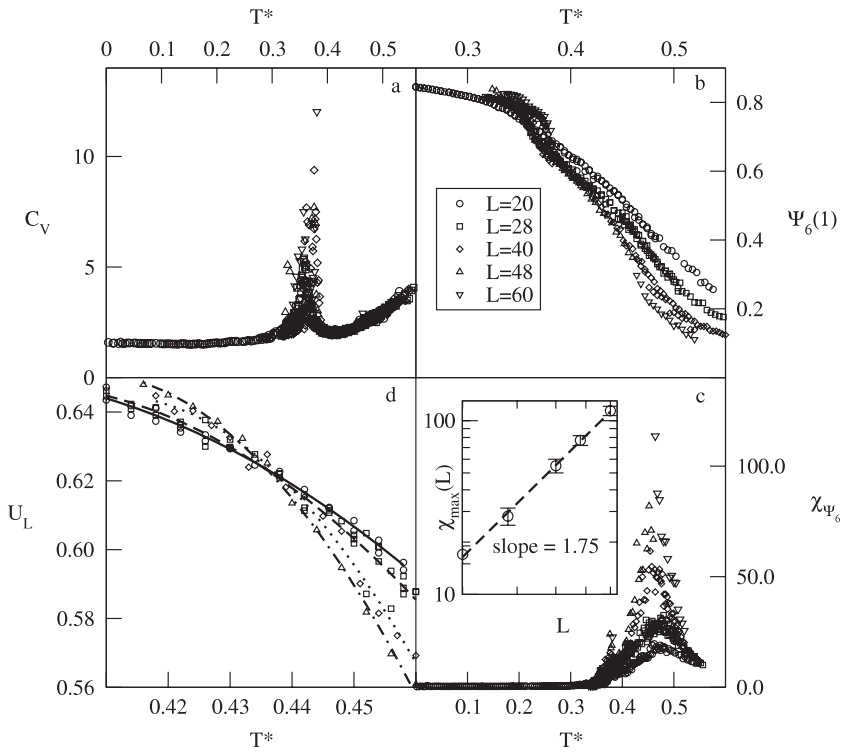

Figure 11. The plots of specific heat (part (a)), bond-orientational order parameter Ψ_6 (part (b)), its susceptibility (part (c)) and fourth-order cumulants (part (d)) versus temperature, for the system with $\sigma^* = 1.27$, $\varepsilon^*_{gs} = 1.0$ and $V_b = 0.5$ and for different sizes of the simulation cell (shown in part (b)). The inset to part (c) shows the log–log plot of the bond-orientational order parameter susceptibility maximum versus the simulation cell size.

strictly two-dimensional. The adsorbed atoms are allowed to displace in the direction normal to the surface, and this may lead to important changes in the mechanism of the melting transition. In particular, even small vertical displacements of adatoms mean that the system may be considered as effectively three-dimensional. As a consequence, the melting may be a first-order rather than a continuous transition. The above statement is supported by the local density profiles recorded at the temperatures below and above the melting point, which have demonstrated that out-of-plane motion of adatoms leads to a slight broadening of the profiles upon melting. It should be emphasized that we have not observed any traces of the second-layer promotion at the temperatures just above the melting point.

It is also possible that the observed sharp heat capacity peaks mark the triple-point melting. The snapshot shown in figure 12(a), which was recorded at the temperature below the melting point, is characteristic for a two-phase region. A dense solid phase coexists with a very dilute gas phase, represented by a void. Upon melting, the system is likely to enter the region in which a solid phase coexists with a liquid (see figure 12(b)). The presence of hexagonally ordered solid regions may be responsible for large values of the bond-orientational order parameter Ψ_6 above the melting temperature. The above scenario is consistent with the prediction that melting occurs via a first-order transition. One should note that our simulations were carried out at constant density, and distinguishing a coexistence region from a hexatic phase is a difficult task. One possibility would be to record the orientational correlation function ($g_6(r) = \langle \Psi_6(r)\Psi_6(0)\rangle$) and check whether it exhibits algebraic decay, as predicted for hexatic phase. In order to obtain reliable results one would need to perform simulations for systems still larger than those considered here.

The inspection of snapshots (figures 12(a) and (b)) and radial distribution functions (figure 13) at the temperatures below and above the melting point demonstrated that the system exhibits hexagonal ordering, below as well as above the melting transition, in agreement with the behavior of the bond-orientational order parameter Ψ_6.

The second transition, which occurs at the temperature of about 0.435, appears to be a continuous transition belonging to the universality class of the two-dimensional Ising model. In particular, the log–log plot of the maximum value of the susceptibility $\chi_{\Psi_6,\max}$ versus L is linear with a slope equal to about 1.75 and the fixed point of the fourth-order cumulant of Ψ_6 occurs at about 0.62. These two values are in a good agreement with the values predicted for the two-dimensional Ising model ($\gamma/\nu = 1.75$ and $U^* = 0.613$) [36].

The presence of the Ising-like transition supports the view that the mechanism of melting is consistent with the theory of Nelson and Halperin [34]. Here we should recall the results of our earlier Monte Carlo study of strictly two-dimensional Lennard-Jones fluid in an external field of square symmetry [37]. For a weakly corrugated surface potential the melting behavior was found to be qualitatively the same as observed here, demonstrating that the above mentioned deviations of monolayer films from planarity do not contribute

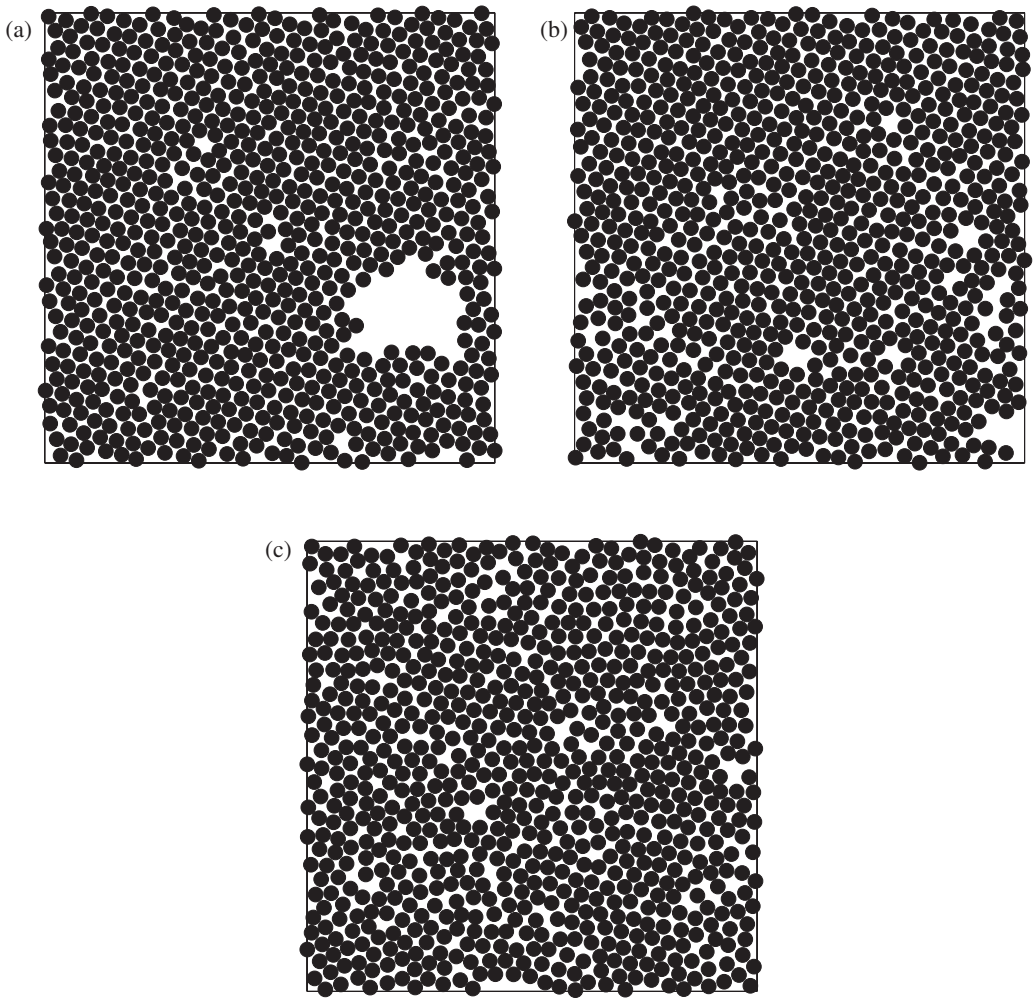

Figure 12. Snapshots of configurations for the system with $\sigma^* = 1.27$, $\varepsilon^*_{gs} = 1.0$ and $V_b = 0.5$ and $L = 40$ recorded at the temperatures $T^* = 0.34$ (part (a)), 0.385 (part (b)) and 0.46 (part (c)).

much to the mechanism of melting. The above seems to support the view that the melting transition occurs according to the mechanism predicted by Nelson and Halperin. Of course, we can not exclude the possibility that melting occurs via a first-order transition.

The results obtained using the grand canonical ensemble simulation are consistent with the presence of two different condensed phases of high degree of triangular ordering. The adsorption–desorption isotherms obtained at different temperatures and for the simulation cell of $L = 28$ (see figure 14) demonstrate that at the temperature of 0.3 the condensation of the dilute gas phase (G) leads directly to the quite well ordered incommensurate floating phase of triangular order (IC_2). At $T = 0.35$, we already observe the presence of two different condensed phases (IC_1 and IC_2), both exhibiting quite a high degree of triangular ordering. This transition is also present at still higher temperatures, but at $T^* \geqslant 0.4$ we also find a disordered liquid-like phase (DL).

From the isotherms we have constructed the phase diagram, shown in the inset to figure 14. It is evident that there are two triple points present. The first triple point, located at the temperature of about 0.31, corresponds to the coexistence between the two incommensurate phases, IC_1 and IC_2, and the dilute gas phase. At the second triple point, located at $T^* \approx 0.395$, the incommensurate phase IC_1, the disordered liquid phase (DL) and the gas phase (G) coexist. The results obtained suggest that the lines corresponding to the phase transitions between the disordered liquid and IC_1 phases and between the two incommensurate phases IC_1 and IC_2 meet at a temperature just below 0.5. The isotherms recorded at the temperatures 0.48 and 0.49 have shown that the phase transition between the disordered liquid and the IC_1 phases is continuous, while a discontinuous transition occurs at the temperature of 0.45. Therefore, a tricritical point is expected to exist at a certain temperature between 0.45 and 0.48.

In the case of slightly larger adsorbate atoms of $\sigma^* = 1.28$, the ground state calculations also do not predict the formation of AT. Although one can find the parameters ε^*_{gs} and V_b for which the AT phase has lower energy than the commensurate phase (see figure 7(a)), nevertheless the incommensurate floating phase of triangular symmetry has an energy still lower than the AT phase one. However, a stable AT ordered phase has been found at non-zero temperatures for the systems characterized by $\varepsilon^*_{gs} = 1.5$ and the corrugation

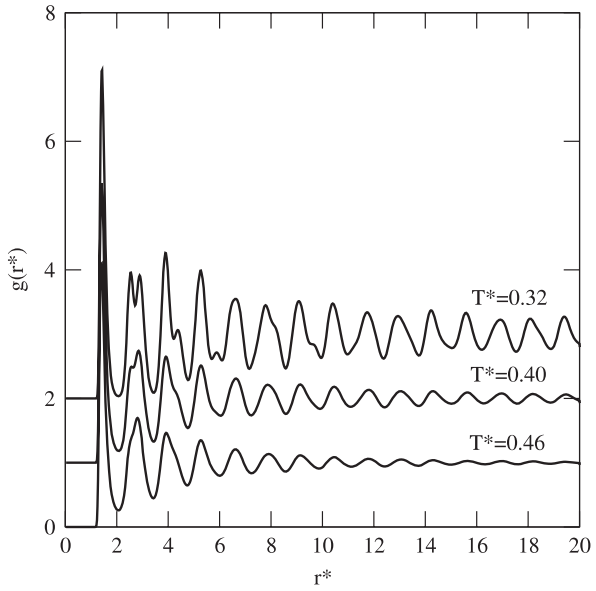

Figure 13. Radial distribution functions for the system with $\sigma^* = 1.27$, $\varepsilon^*_{gs} = 1.0$ and $V_b = 0.5$ and $L = 40$ recorded at different temperatures (shown in the figure). Note that the plots are shifted for clarity.

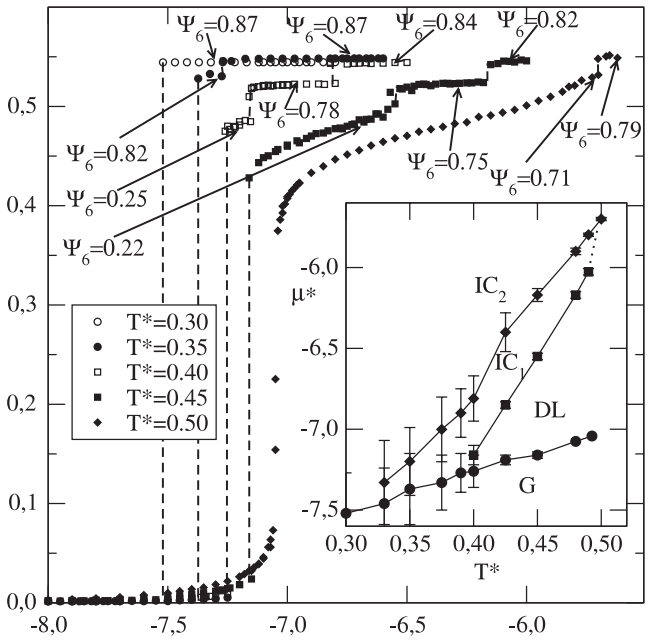

Figure 14. The adsorption–desorption isotherms for the system with $\sigma^* = 1.27$, $\varepsilon^*_{gs} = 1.0$ and $V_b = 0.5$ and $L = 40$ recorded at different temperatures: $T^* = 0.30$ (open circles), 0.35 (filled circles), 0.40 (open squares), 0.45 (filled squares) and 0.5 (filled diamonds). The values of the bond-orientational order parameter Ψ_6 at selected values of the chemical potential correspond to different condensed phases. The inset shows the phase diagram, in the μ^*–T^* plane, for the same system.

parameter $V_b = 0.5$ and 0.55. For $V_b = 0.45$ the system exhibits triangular order, while for $V_b = 0.6$ only the commensurate phase appears. This was demonstrated by the behavior of the order parameters, the radial distribution functions, as well as from the inspection of snapshots.

For σ^* between 1.29 and 1.44, the AT phase is predicted to be stable already at zero temperature when the strength of surface potential and its corrugation are both suitably chosen (cf figure 7). The results of ground state calculations for the systems characterized by $\sigma^* = 1.29$, $\varepsilon^*_{gs} = 1.50$ and different values of the corrugation parameter V_b have shown (see figure 7(b)) that the AT should be stable at zero temperature over a narrow range of V_b between about 0.475 and 0.485. Finite temperature canonical ensemble Monte Carlo simulation performed at the density $\rho = 0.5$ have demonstrated, however, that the AT phase remains stable at still lower values of V_b equal to 0.46 and 0.44, indicating again that our ground state calculations for the triangularly ordered phase overestimate its stability. This can be attributed to the fact that the density considered is lower than the density of fully filled triangular phase. On the other hand, grand canonical simulations carried out for $V_b = 0.46$ have demonstrated that only the phase of triangular order is stable at sufficiently low temperatures, confirming the predictions stemming from the ground state calculations.

Now, we shall consider a series of systems with $\sigma^* = 1.30$ and address the problem of the influence of the surface potential curvatures (k_x and k_z) on the stability of AT phase. We have chosen a series of systems (see table 1) for which the commensurate phase is stable at zero temperature, but the AT phase develops at finite temperatures. The systems 1–4 from table 1 are characterized by roughly the same potential barrier for diffusion ($V^*_D \approx 0.76$) and by different curvatures of the surface potential k_x and k_z. Figure 15

Table 1. The parameters characterizing the systems with $\sigma^* = 1.30$.

No.	ε^*_{gs}	V_b	V^*_D	k_x	k_z
1	1.55	0.60	0.763	8.217	155.0
2	1.00	0.80	0.767	9.239	100.6
3	3.10	0.35	0.760	7.478	306.1
4	0.65	1.00	0.765	10.83	64.1
5	0.55	1.00	0.647	9.167	54.3
6	3.20	0.40	0.922	9.159	317.1
7	2.35	0.50	0.901	9.289	234.0
8	1.50	0.65	0.826	9.159	150.5

presents the temperature changes of the bond-orientational order parameters Ψ_4 (part (a)) and Ψ_{12} (part (b)) of the specific heat (part (c)) and of the order parameter $|\rho_q|$ (part (d)) for these four systems. Two important features are clearly seen. The temperature at which the commensurate phase transforms into the AT phase increases nearly linearly with k_x (see figure 16(a)). It should be noted that the magnitude of k_z changes in a reverse order to k_x for the systems considered, so that one might conclude that the temperature at which the transition between c(2×2) and AT phases takes place decreases when k_z becomes higher. This is not likely to be the case, as will be demonstrated soon.

On the other hand, the temperature at which the AT disorders is primarily determined by the magnitude of k_z, and increases with k_z (see figure 16(a)). It should be also noted that the disordering temperature of the AT phase for the systems 2, 5–8, for which the magnitude of k_x is nearly the same, changes with k_z in a similar way (see figure 16(b)). Of course, the

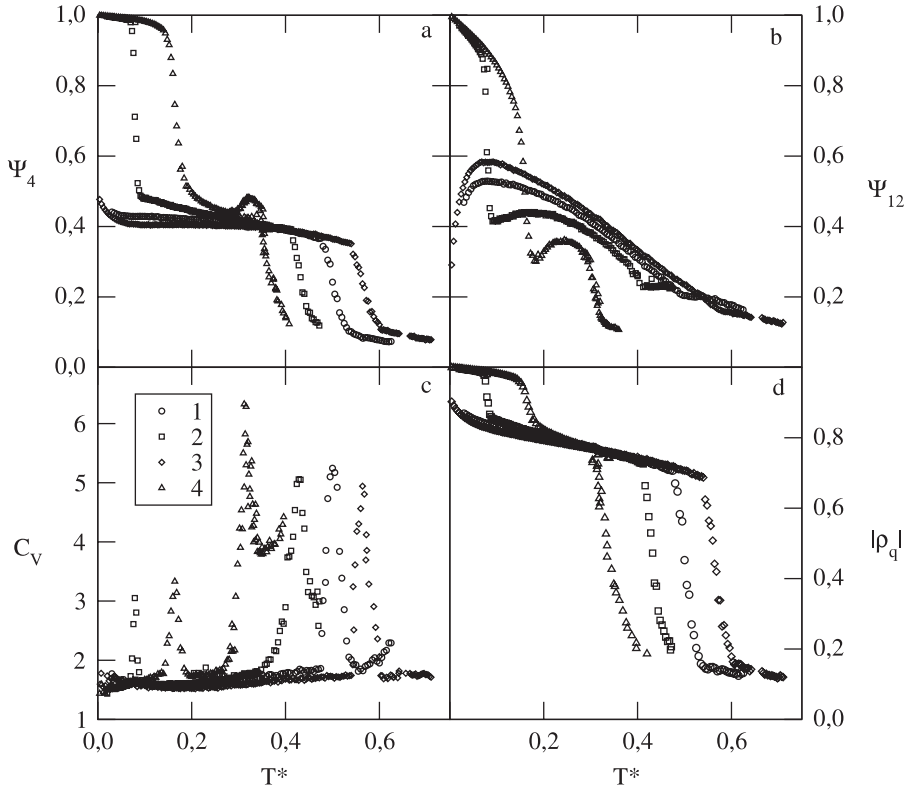

Figure 15. The plots of the bond-orientational order parameters ψ_4 (part (a)) and Ψ_{12} (part (b)) of the specific heat (part (c)) and the order parameter $|\rho_q|$ (part (d)) versus temperature for the systems 1, 2, 3 and 4 from table 1.

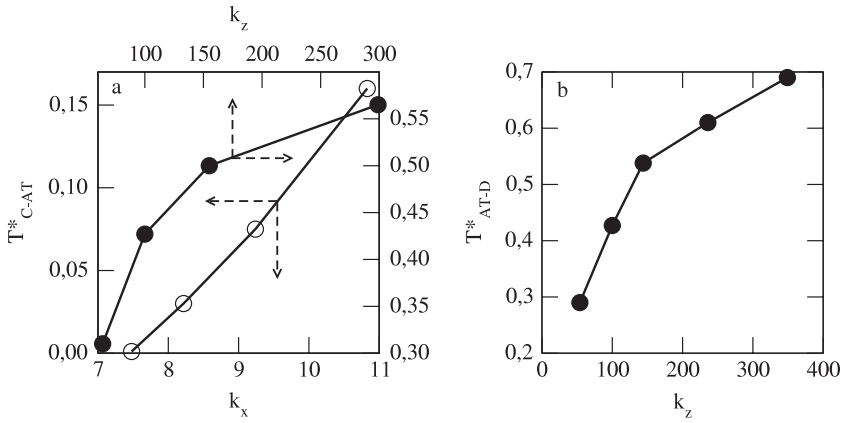

Figure 16. Part (a) shows the changes of the temperatures of the phase transition between the commensurate c(2 × 2) and AT phases versus the surface potential curvature k_x (open circles) and of the temperatures of the phase transition between the AT and disordered phases versus the surface potential curvature k_z (filled circles) for the systems 1, 2, 3 and 4 from table 1. Part (b) is the plot of the temperatures of the phase transition between the AT and disordered phases versus the surface potential curvature k_z for the systems 2, 5, 6, 7 and 8 from table 1.

magnitude of the curvature k_z also influences the transition between the commensurate phase and the AT phase, but not in a way suggested by the results obtained for systems 1–4. One expects that the stability of the commensurate phase should be enhanced by higher values of k_z, due to a decreased ability of out-of-plane displacement of adatoms from the registry positions. Indeed, our Monte Carlo calculations performed for the systems 2, 5–8 from table 1 confirm that prediction quite well. Figure 17 presents the plots of the bond-orientational order parameters Ψ_4 and Ψ_{12} versus temperature, which demonstrate that the temperature at which the transition between the commensurate c(2 × 2) structure and the AT phase takes place is shifted towards higher temperatures when k_z increases. This figure also shows that the potential barrier for diffusion considerably influences the behavior of the film. The systems 2 and 5, which are characterized by lower potential barriers for diffusion than the systems 6, 7 and 8, exhibit the formation of AT phase, while the systems 6 and 7 with the two highest values of the potential barrier do not exhibit the formation of AT. The system 8, with the intermediate values of

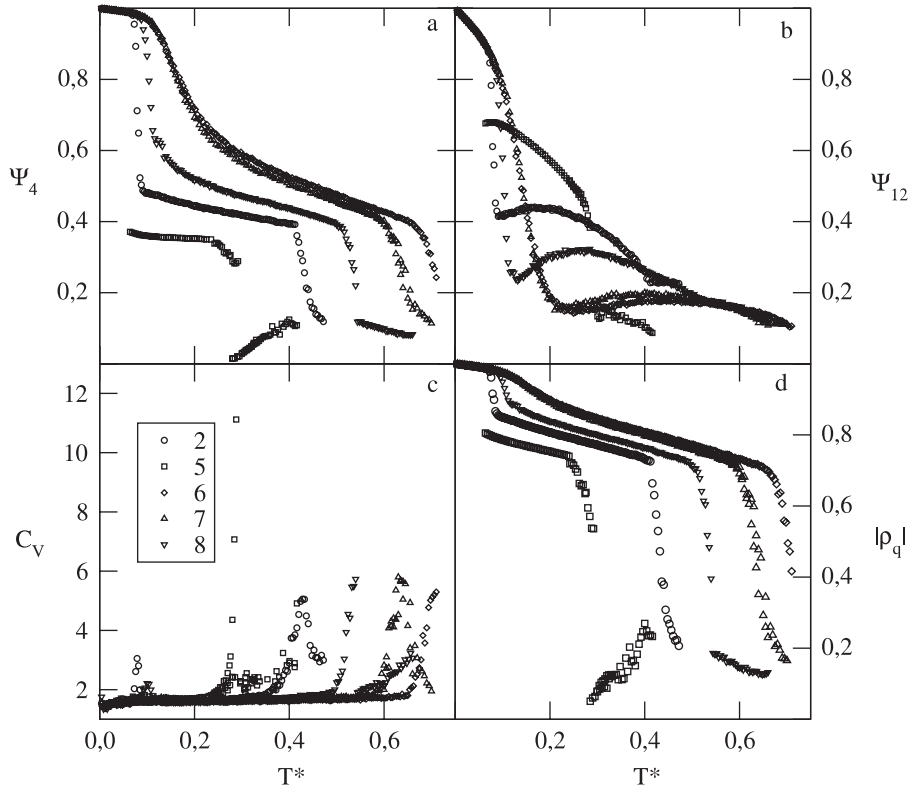

Figure 17. The plots of the bond-orientational order parameters ψ_4 (part (a)) and Ψ_{12} (part (b)) of the specific heat (part (c)) and the order parameter $|\rho_q|$ (part (d)) versus temperature for the systems 2, 5, 6, 7 and 8 from table 1.

both k_z and V_D^*, orders into the AT at the temperatures between about 0.19 and 0.54. The density distribution functions as well as the snapshots for the systems 6 and 7 have not shown the development of AT phase at all.

The behavior of systems with σ^* up to 1.44 is qualitatively similar to the above discussed cases and the AT appears at the ground state or at finite temperatures, depending on the surface potential properties. Figure 18 presents a sort of phase diagram, which shows the temperature regions over which different condensed phases are stable plotted versus the surface potential curvature k_x, for a series of systems of adsorbate atoms with $\sigma^* = 1.34$ and the surface potential characterized by $V_b = 1.0$ and by different strength (ε^*_{gs}). Of course, the surface potential curvatures, k_x and k_z, are both proportional to the surface potential strength ($k_x = 16.226\varepsilon^*_{gs}$ and $k_z \approx 98\varepsilon^*_{gs}$). The results obtained demonstrate that the disordering of the AT phase occurs via a first-order phase transition, no matter whether it leads to the formation of the ordered fluid-like (OF) phase of square symmetry or to the floating incommensurate phase of triangular symmetry (HEX).

Finite temperature simulations performed for a series of systems characterized by the same values of $\varepsilon^*_{gs} = 1.0$ and $V_b = 1.0$ but with different σ^* between 1.33 and 1.38 have confirmed the ground state prediction that for $\sigma^* > 1.36$ the AT phase should be stable already at the ground state (cf figure 4), as well as the prediction that for $\sigma^* = 1.39$ the stable phase at low temperatures should be the floating incommensurate phase of triangular order. The results shown in figure 19 demonstrate that a gradual increase of σ^* from 1.34 to 1.38 leads to an increase of the bond-orientational order parameter Ψ_6 in the phase resulting from the disordering of the AT phase. This partially ordered phase undergoes a continuous phase transition to a liquid-like disordered phase

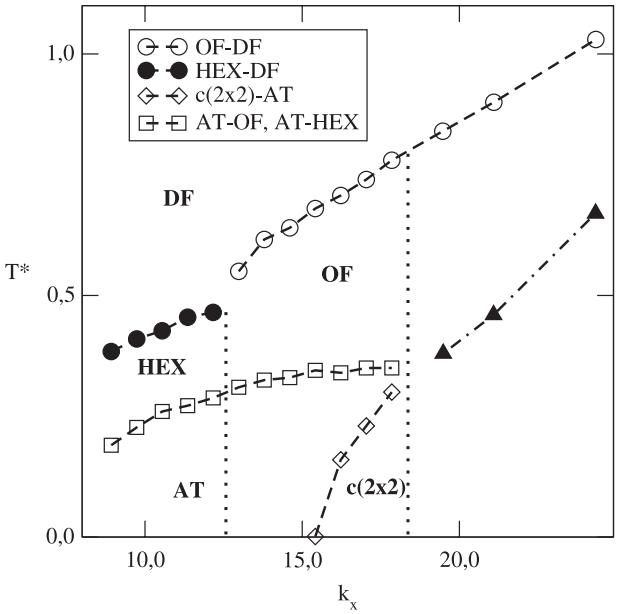

Figure 18. The stability regions of different phases for the systems characterized by $\sigma^* = 1.34$, the corrugation parameter $V_b = 1.0$ and different values of ε^*_{gs} plotted against the surface potential curvature k_x.

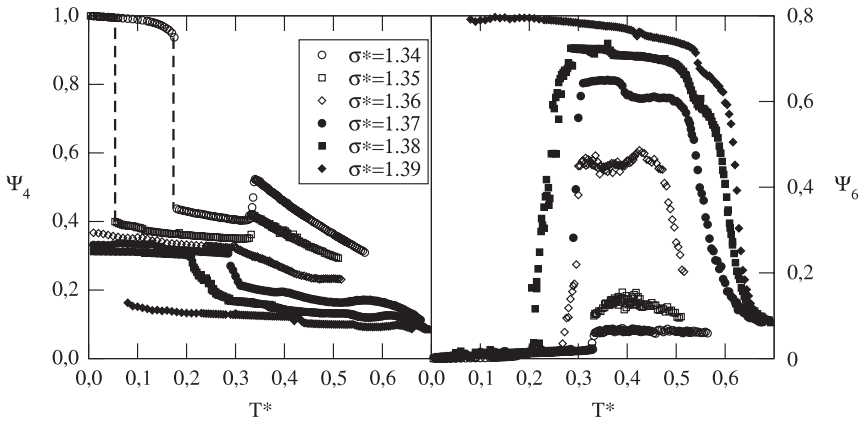

Figure 19. The plots of the bond-orientational order parameters ψ_4 (left panel) and Ψ_6 (right panel) for a series of systems characterized by $\varepsilon^*_{gs} = 1.0$, $V_b = 1.0$ and different σ^* (shown in the figure).

upon a further increase of temperature. This transition belongs to the universality class of the two-dimensional Ising model, as already demonstrated for the systems with $\sigma^* = 1.27$.

For the atoms of $\sigma^* = 1.45$ the adatom–adatom interaction becomes already weakly repulsive when the film is ordered into a perfect c(2 × 2) commensurate structure, but becomes attractive upon the displacement of adatoms leading to the formation of AT phase. Of course, the displacement of adatoms from the registry positions is always accompanied by a decrease of the adatom–surface interaction energy. Nevertheless, in the case of systems with sufficiently low curvatures of the surface potential the displacement of adatoms may favor the formation of AT phase rather than the floating incommensurate phase of triangular ordering. Of course, when the size of adatoms becomes large enough the monolayer film of the density corresponding to a perfect commensurate c(2 × 2) phase becomes unstable and the system relaxes to a more stable state, in which a certain fraction of atoms are transferred to the second layer. Such promotion of the second layer has been observed for the system with $\sigma^* = 1.47$ and even with rather strong surface potential, characterized by $\varepsilon^*_{gs} = 3.0$ and $V_b = 1.0$. Despite a high potential barrier between adjacent sites ($V^*_D \approx 3.09$) the resulting structure has a well developed triangular symmetry (see figure 20). Also the atoms promoted to the second layer form a cluster of triangular ordering.

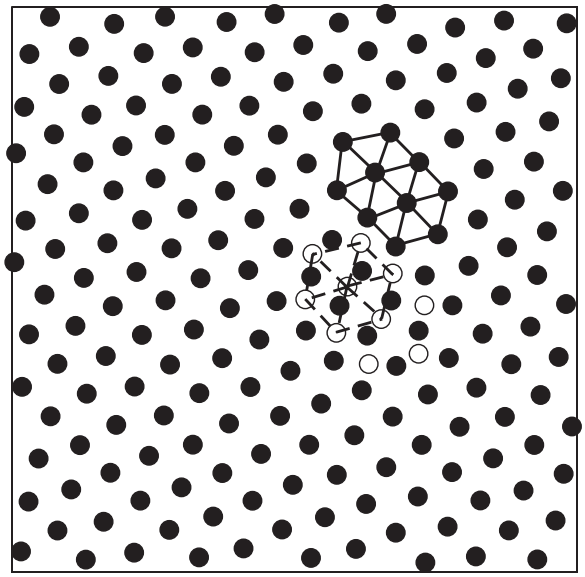

Figure 20. The snapshot of the configuration for the system with $\sigma^* = 1.47$, $\varepsilon^*_{gs} = 3.0$, $V_b = 1.0$, recorded at $T^* = 0.03$ and $L = 20$. The atoms in the first (second) layer are shown as filled (open) circles).

5. Summary and conclusions

In this work we have discussed the mechanism leading to the development of Archimedean tiling of the type (3^2.4.3.4) in monolayer films formed by Lennard-Jones atoms on surfaces of square symmetry. Ground state calculations have demonstrated that Archimedean tiling may exist already at $T = 0$. Finite temperature Monte Carlo simulation results have been found to be in a good agreement with the predictions stemming from the ground state calculations. It has been shown that the stability of AT structure strongly depends on the curvatures of the holding potential.

Moreover, we have obtained rather convincing evidence that the melting of hexagonally ordered floating incommensurate phase formed on the substrate of square symmetry occurs via two phase transitions, in agreement with the predictions stemming from the theory of Nelson and Halperin. The first transition does not affect the hexagonal ordering of the film much. However, our results have demonstrated that this transition is accompanied by a well developed heat capacity anomaly, not predicted to occur for the system undergoing defect mediated melting. The second transition has been demonstrated to be continuous and belonging to the universality class of the two-dimensional Ising model, just as predicted by Nelson and Halperin.

Concluding, we should mention the question of a possible development of AT ordering in bilayer films. In general, attempts to obtain bilayer films with AT structure in either the top or in both layers were not successful. Of course,

the presence of the second layer stabilizes the commensurate structure in the layer adjacent to the solid substrate, as already discussed in one of our previous papers [15]. It was also demonstrated that for the system of $\sigma^* = 1.34$, $\varepsilon_{gs} = 1.0$ and $V_b = 1.0$, the second layer assumes the structure in which commensurate domains are separated by highly localized walls running along the diagonal of the surface lattice symmetry axes. Quite similar structures have been observed for systems of still larger atoms of σ^* between 1.35 and 1.38. Our conclusion is that the AT ordering is not likely to appear in bilayer as well as in thicker films due to enhanced stability of the commensurate phase in layers adjacent to the solid surface and a fast decay of the corrugation potential with the distance from the surface.

Acknowledgments

The authors would like to thank Dr Kurt Binder for stimulating discussions. This work was supported by the EC under the grant No. MTDK-CT-2004-509249.

References

[1] *Films on Solid Surfaces* 1975 (New York: Academic)
[2] Taub H, Torzo G, Lauter H J and Fain S C Jr (ed) 1991 *Phase Transitions in Surface Films 2* (New York: Plenum)
[3] Bruch L W, Cole M W and Zaremba E 1997 *Physical Adsorption: Forces and Phenomena* (Oxford: Clarendon)
[4] Patrykiejew A, Sokołowski S and Binder K 2000 *Surf. Sci. Rep.* **37** 207
[5] Park R I and Madden H H 1968 *Surf. Sci.* **11** 188
[6] Kern K, Zeppenfeld P, David R and Comsa G 1987 *Phys. Rev. Lett.* **59** 79
[7] Weimer W, Knorr K and Wiechert H 1988 *Phys. Rev. Lett.* **61** 1623
[8] Ramseyer C, Pouthier V, Girardet C, Zeppenfeld P, Büchel M, Diercks V and Comsa G 1997 *Phys. Rev.* B **55** 13203
[9] Zeppenfeld P, Becher U, Kern K and Comsa G 1992 *Phys. Rev.* B **45** 5179
[10] den Nijs M 1988 *Phase Transitions and Physical Phenomena* vol 12, ed C Domb and J L Lebowitz (London: Academic) p 219
[11] Patrykiejew A, Sokołowski S and Binder K 2002 *Surf. Sci.* **512** 1
[12] Novaco A D and McTague J P 1977 *Phys. Rev. Lett.* **38** 1286
[13] McTague J P and Novaco A D 1979 *Phys. Rev.* B **19** 5299
[14] Leatherman G S, Diehl R D, Karimi M and Vidali G 1997 *Phys. Rev.* B **56** 6970
[15] Patrykiejew A and Sokołowski S 2007 *J. Phys. Chem.* C **111** 15664
[16] Patrykiejew A and Sokołowski S 2007 *Phys. Rev. Lett.* **99** 156101
[17] Suck J-B, Schreiber M and Häusller P (ed) 2002 *Quasicrystals: An Introduction to Structure, Physical Properties and Applications* (Berlin: Springer)
[18] Schmiedeberg M and Stark H 2008 *Phys. Rev. Lett.* **100** 019601
[19] Grünbaum B and Shepard G C 1987 *Tilings and Patterns* (New York: Freeman)
[20] Bergman G and Shoemaker D P 1954 *Acta Crystallogr.* **7** 857
[21] Frank F C and Kasper J S 1959 *Acta Crystallogr.* **12** 483
[22] Zeng X, Unger G, Liu Y, Percec V, Dulcey A E and Hobbs J K 2004 *Nature* **428** 157
[23] Takano A, Kawashima W, Noro A, Isono Y, Tanaka N, Dotera T and Matsushita Y 2005 *J. Polym. Sci.* B **43** 2427
[24] Steele W A 1973 *Surf. Sci.* **36** 317
[25] Kim H-Y and Steele W A 1992 *Phys. Rev.* B **45** 6226
[26] Tesi M C, van Rensburg E J, Orlandini E and Whittington S G 1996 *J. Stat. Phys.* **82** 155
[27] Hansmann U H E 1997 *Chem. Phys. Lett.* **281** 140
[28] Strandburg K J 1988 *Rev. Mod. Phys.* **60** 161
[29] Vishnyakov A and Neimark A V 2003 *J. Chem. Phys.* **118** 7585
[30] Rapaport D C 1995 *The Art of Molecular Dynamics Simulation* (Cambridge: Cambridge University Press)
[31] Binder K 1995 *Cohesion and Structure of Surfaces* vol 4, ed F R De Boer and D G Pettifor (Amsterdam: Elsevier)
[32] Landau D P and Binder K 2000 *A Guide to Monte Carlo Simulation in Statistical Physics* (Cambridge: Cambridge University Press)
[33] Patrykiejew A, Sokołowski S, Zientarski T and Binder K 1995 *J. Chem. Phys.* **102** 8221
[34] Nelson R D and Halperin B I 1979 *Phys. Rev.* B **19** 2457
[35] Kosterlitz M and Thouless P J 1973 *J. Phys. C: Solid State Phys.* **6** 1181
[36] Kamieniarz G and Blöte H W J 1993 *J. Phys. A: Math. Gen.* **26** 201
[37] Patrykiejew A, Zientarski T and Binder K 1996 *Acta Phys. Pol.* **89** 308